***JKPK (JURNAL KIMIA DAN PENDIDIKAN KIMIA)**, Vol. 6, No. 2, 2021* *pp. 192-205*
Chemistry Education Study Program, Universitas Sebelas Maret *ISSN 2503-4146*
https://jurnal.uns.ac.id/jkpk *ISSN 2503-4154 (online)*

REMAZOL BRILIANT BLUE UPTAKE BY GREEN AND LOW-PRICE BLACK CARBON FROM ILALANG WEEDS (*Imperata cylindrica*) ACTIVATED BY KOH SOLUTION

Ngatijo[1,*], Edwin Permana[1], Lusi Pitri Yanti[1], Bayu Ishartono[2], and Rahmat Basuki[2,3]

[1] Department of Chemistry, Faculty of Science and Technology, Universitas Jambi,
Jl. Jambi - Muara Bulian No.KM. 15, Muaro Jambi, Jambi Province, Indonesia, 53631

[2] Bureau of School Curriculum Analysis, Design, and Interpretation, Master of Chemistry Alumny Forum (FAMK), Universitas Gadjah Mada,
Sekip Utara Bulaksumur, Sleman District , Special Region of Yogyakarta, Indonesia 55281

[3] Department of Chemistry, Faculty of Military Mathematics and Natural Sciences, Universitas Pertahanan RI
IPSC Sentul Area, Bogor, West Java, Indonesia 16810

* correspondence tel/fax : 821-8581-3527, email: tijo52@yahoo.co.id

Received: July 31, 2021 Accepted: August 23, 2021 Online Published: August 27, 2021
DOI : 10.20961/jkpk.v6i2.53113

ABSTRACT

The synthesis of activated carbon (AC) from green, low-price, and renewable sources as a pollutant adsorbent is the growing interest of researchers. This work aims to synthesis of AC from Ilalang weed (*Imperata cylindrica*) (IW-AC) with KOH activator as a green and low price Remazol Brilliant Blue dye (RBB) adsorbent. The success of IW-AC synthesis was characterized by Fourier Transform-Infrared (FT-IR) and Scanning Electron Microscopy (SEM). The effects of initial solution pH, adsorbent dosage, initial RBB concentration, and contact time were systematically investigated. Results showed the optimum condition of RBB adsorption occurred at low pH (2.0-4.0) and 75 mg of adsorbent dosage. Under the optimum condition, the equilibrium adsorption data fitted well to the Langmuir isotherm with the adsorption capacity of RBB uptake was 13.42 mg/g. Calculation of adsorption energy by Dubinin-Radushkevich (D-R) isotherm model (13.39 kJ/mol) showed that the electrostatic interaction was the main interaction of RBB adsorption on IW-AC. Adsorption kinetics showed that the adsorption behaviour followed the Ho pseudo-second-order kinetic model. The experimental results of this work demonstrate that the IW-AC can be used as a promising green and low-cost adsorbent for the removal of anionic dyes from an aqueous solution.

Keyword: Adsorption, Green and low-price adsorbent, Ilalang weed-activated carbon, Remazol brilliant blue uptake, KOH activator

INTRODUCTION

Dyes are the essential material for dyeing fabrics in the textile industry. The use of dyes in the fabric dyeing process is the major contributor to liquid waste wasted in aquatic ecosystems [1]. The use of commercial textile dyes such as Remazol Brilliant Blue (RBB) is widely applied in the dyeing process because it has a chromophore group that contributes to a bright blue color to the fabric fiber and is not easy to be degraded. RBB dye possesses six

to ten benzene rings of anthraquinone structure that make it highly stable, difficult to degrade biologically, and resistant to chemical oxidation reactions [2]. As a result, pollution due to Remazol Brilliant Blue dye in aquatic ecosystems can cause serious health problems such as irritation to the eyes, skin, respiration, and digestion and stimulate the growth of cancer cells [3].

Various methods have been developed to reduce the pollution caused by the disposal of dye liquid waste from the dyeing process in the textile industry, including wastewater electrolysis [4], ionic exchange [5], photodegradation [6][7], membrane exchange [8], and biodegradation using plants, as well as adsorption [9][10]. The use of adsorbents via the adsorption method has grown in popularity because the system is simple, environmentally friendly, and cost-effective [11], [12]. The development of cellulose-based adsorbent materials in the form of activated carbon (AC) for the uptake of metal ions and dyes has been widely reported [13][14][15]. AC is an amorphous material that can obtain larger porosity and higher surface area by acid or alkaline activator [16]. These improvements make AC to be promising adsorbent for pollutant handling.

Recently, the production of AC from green, low-price, and renewable sources is growing researchers' interest [17]. The AC source that has been reported include cassava leaves [18], rubber fruit shell [19], Sengon wood (*Paraserianthes falcataria*) shaws powder [20], sugarcane dregs [21], Durian peel [22], coconut shell [23], and Enceng Gondok plant [24]. One of the abundant plants, high availability, and cheap is Ilalang Weeds (*Imperata cylindrica*).

Ilalang Weeds (*Imperata cylindrica*) are reported to contain relatively high cellulose, hemicellulose, and lignin [16]. However, the literature has limitedly found the utilization of Ilalang Weeds (Imperata cylindrical) as a carbon source that is activated by an activator [13]. Therefore, this study aims to utilize Ilalang Weeds (*Imperata cylindrical*) as a source of AC for RBB uptake. The activator used in this work is KOH that have been previously reported as an effective impurities removal activator to acquire large pore and high surface area of AC [25,26,27,28]. Further, the optimum uptake condition, isotherm, and kinetics study are critically discussed in this paper.

METHODS

1. Materials

The main materials used in this study were the Ilalang Weeds (*Imperata cylindrica*) from the Mendalo area, Muaro Jambi Regency, Jambi, Indonesia. *Imperata cylindrica* sample was prepared in advance by cleaning from impurities, washing, cutting into small pieces, and then drying under the sun. Merck's pro analyst chemicals used in this study include potassium hydroxide (KOH), nitric acid (HNO_3), sodium hydroxide (NaOH), and Remazol Brilliant Blue dye.

2. Instruments

The preparation equipment used in this study included mortar and pestle grinder, 80 mesh Fischer siever, Mettler AE 100 analytical balance, spatula, IKA C-MAG HS 4 magnetic stirrer, micropipette, Mettler Toledo pH meter, Ney Vulcan 3-550 furnace, DLAB MS H280 Pro magnetic stirrer, and Memmert oven.

Several analytical instruments used included the Perkin Elmer Lambda 35 UV-Vis Spectrophotometer (Jambi Province Quality Testing and Certification Laboratory), Perkin Elmer Frontier Infrared Spectrometer (FTIR) (MIPA Laboratory, Padang State University), and Hitachi Flexsem 1000 Scanning Electron Microscope (SEM) (Department of Mechanical Engineering, Sepuluh Nopember Institute of Technology, Surabaya).

3. Activated Carbon Synthesis

According to a modified previous study, the process of producing cellulose-based activated carbon from Imperata cylindrica was carried out in 2 stages: carbonization and activation processes [29]. In the carbonization stage, several *Imperata cylindrica* were heated using a furnace at a temperature of 300 °C for 2 h to form carbon powder. Then, the carbonization results were ground and sieved using an 80 mesh sieve.

In the activation stage, a mass of carbon resulting from the carbonization stage was added with 10% KOH solution ($^{w}/_{v}$), stirred using a magnetic stirrer for 1 h, and left for 24 h at room temperature. After activation, the activated carbon was filtered and washed with double distilled water to a neutral pH, then dried in an oven at 105 °C for 2 h. Finally, the prepared Ilalang Weeds activated carbon (IW-AC) was characterised using FTIR and SEM.

4. Optimum Adsorption Condition: Influence of pH and Mass of Adsorbent

The influence of pH was carried out by filling five glass beakers (50 mL capacity) with 40 mL of RBB 15 ppm solution. The HNO3 and KOH were dropped into each beaker to adjust the pH in the range of 2.0 to 8.0. All of the RBB adjusted pHs was divided into 2 (20 mL each). The 0.1 g of AC was added into five series adjusted pH as a sample and the other series adjusted pH as control. The sample was then shaken at 250 rpm for 3 h. UV-Vis examined the filtrate at a wavelength of 632 nm to quantify the amount rest of RBB. The adsorbed RBB is calculated by Equation 1, where q_e is the adsorbed RBB at equilibrium (mg/g), C_0 is the initial RBB concentration (ppm), C_e is the RBB concentration at equilibrium (mg/L), V is the volume of RBB (L), and m is mass of the AC (g). The highest adsorbed RBB proclaimed as the optimum pH.

$$q_e = \frac{(C_0 - C_e)V}{m} \quad (1)$$

The effect of adsorbent mass was carried out by adding the five variations of mass of AC: 25, 50, 75, 100, and 125 mg into 20 mL RBB 15 ppm. The mixture was shaken at 250 rpm for 3 h. The solution was filtered, and the filtrate was analyzed by UV-Vis spectrophotometer at a wavelength of 632 nm for each treatment.

5. Kinetics Study

Kinetics study was conducted by variation of contact time. Into the six glass beaker (50 mL capacity) the 20 mL of RBB 15 ppm solution and 0.075 g of IW-AC was added. The mixture was then shaken at 250 rpm for desired contact time (15, 30, 45, 60, 90, and 120 min). The mixture was then filtered, and the filtrate was analyzed with a UV-Vis spectrophotometer at a wavelength of 632 nm for each treatment. The adsorbed RBB at desired time is calculated by Equation 1.

6. Isotherm Study

Isotherm study was conducted by variation of initial RBB concentration. Into the six glass beaker (50 mL capacity), the 20 mL of RBB 15 ppm solution and 0.075 g of IW-AC was added. The mixture was then shaken at 250 rpm for desired initial RBB concentration (10, 20, 30, 40, 60, 80, and 100 ppm). The mixture was then filtered, and the filtrate was analyzed with a UV-Vis spectrophotometer at a wavelength of 632 nm for each treatment. The adsorbed RBB at desired initial RBB concentration is calculated by Equation 1.

RESULTS AND DISCUSSION

1. Preparation of IW-AC

The production of IW-AC was carried out in 2 stages: carbonization and activation. The carbonization stage was conducted by cleaning impurities, washing, cutting into pieces, and drying the Ilalang Weeds. The result of the dry piece Ilalang Weed was presented in Figure 1(a). The carbonization process was carried out using a furnace at a temperature of 300 ºC for 2 h referred to in a previous study [29]. This treatment decomposes the components in *Imperata cylindrica* such as cellulose, hemicellulose, and lignin into carbon by evaporating the volatile non-carbon material. The carbonization process is incomplete combustion with a limited supply of oxygen to produce carbon in the form of charcoal according to the following equations reaction [13]:

$$C_nH_{2n+2(s)}+O_{2(g)} \rightarrow nCO_{(g)}+(n+1)H_2O_{(g)} \quad (2)$$

$$C_nH_{2n+2(s)} + O_{2(g)} \rightarrow nC_{(s)} + (n+1)H_2O_{(g)} \quad (3)$$

In the carbonization process, the decomposition mechanism of the content of lignin, α-cellulose, and hemicellulose to form a carbon occurred in several stages as temperature rises. At a temperature of 100-120 ºC, water evaporation occurred, and cellulose decomposition continued at a temperature of 270 ºC. The exothermic reaction of intensive cellulose decomposition in the form of a solution of pyrolignate, wood gas (CO and CO_2), and a small amount of tar occurred at a temperature of 270-310 ºC. An increase follows the decomposition of lignin in the amount of tar, and a decrease in the pyrolignate solution occurs at a temperature of 310-500 ºC [30]. Meanwhile, the increase in temperature above 500 ºC caused carbon purification to obtain pure carbon content. However, the resulting carbon material has a relatively small pore size because it contains impurities that cove the pore surface, so it is necessary to continue the activation stage.

Figure 1. (a) dry piece Ilalang Weed; (b) physical appearance of IW-AC

Chemical activation was carried out using a 10% KOH solution ($^{w}/_{v}$) to remove impurities such as volatile and tar. KOH as an activating agent can keep the sample from burning by reacting with the mineral content in the raw material to prevent ash formation [31]. Chemical activation using KOH involves the following chemical equation [32]:

$H_2O(l) + C(s) + 2KOH\ (aq) \rightarrow K_2CO_3(aq) + H_2(g)$ (4)

Previous studies explained that the reaction between carbon and KOH produces a K_2CO_3 compound due to the reaction between the activator and CO_2 gas obtained during chemical activation [26][32]. The reaction can also release water because KOH is a dehydrating agent. Carbon reacts with KOH during the activation process, causing the carbon surface to slowly erode, forming holes, resulting in new pores that were not formed in the carbonization stage. The formation of pores also enlarges the surface area of the prepared activated carbon. The physical appearance of synthesized IW-AC was presented in Figure 1(b).

2. Characterization of IW-AC

The analysis of the functional groups contained in the IW-AC was carried out with the help of an infrared spectrometer instrument. Identification of functional groups was conducted by interpreting the absorption in the wavenumber 4000 - 400 cm^{-1}. The results of the characterization of activated carbon functional groups are displayed in Figure 2.

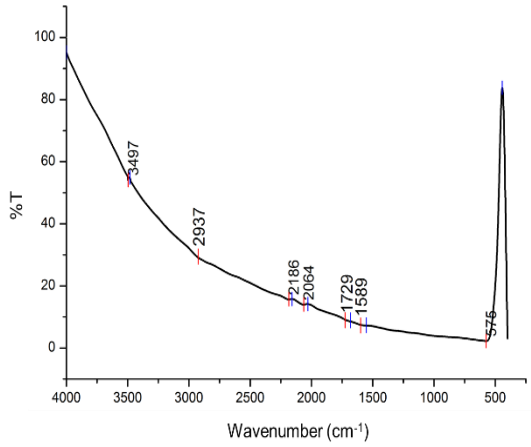

Figure 2. FT-IR spectrum of IW-AC

As seen in Figure 2, IW-AC had absorption at wavenumbers of 3497, 2937, 2186, 1729, 1589, and 575 cm^{-1}. The band at 3497 cm^{-1} was attributed to the O–H stretching vibration of the carboxylate, phenol, or alcohol. The band at 2937 cm^{-1} is in the range of 3000–2850 $cm^{-1,}$ indicating an aliphatic C–H functional group. The band at 2186 cm^{-1} was assigned to C≡C stretching vibration [33]. The presence of carbon with triple bonds (C≡C) indicates that the carbon produced has a high purity where the element of O or H is released, which initially combines with element C. The band at 1729 cm^{-1} was associated with C=O stretching vibration. Aromatic C=C bonds at 1558–1580 cm^{-1} were the constituents of the hexagonal structure of activated carbon. At the same time, the band at 438–815 cm^{-1} referred to C–H vibrations from aromatic compounds [34].

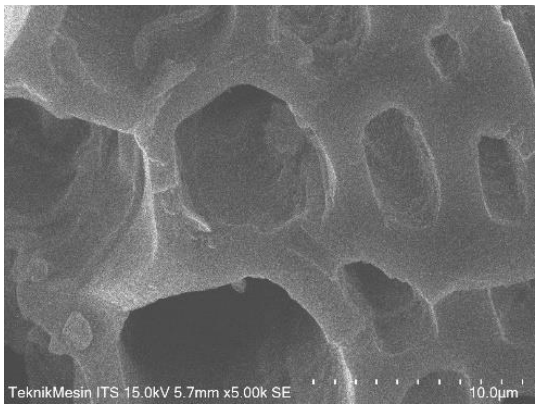

Figure 3. TEM image of IW-AC (5000× magnitude)

The characterization using Scanning Electron Microscope (SEM) aimed to analyze the surface morphology and the differences in the microstructure of the IW-AC. The characterization results showed the material's morphology with the magnification of 5000 times (Figure 3). The surface morphology of

the IW-AC shows pores on the surface due to the activation process using the KOH activator. Based on a previous study, the surface of the adsorbent activated by KOH showed that the KOH had eliminated the ash and tar on the adsorbent surface [27]. Furthermore, it was affected to provide an enter close for the migration of adsorbate molecules onto the active site of the adsorbent. This indicates that the activated carbon can be an adsorbent for RBB dye because it has relatively abundant and large pores. It is possible because the activator plays an important role in removing the remaining volatiles and tar. The carbon is completely pure, and the surface area is even greater [15]. In addition, the pores of activated carbon are included in the macropore structure with a size of 1.55 – 11.31 µm.

3. Optimum Adsorption Condition

pH is an important factor that affects the adsorption process. The pH condition of the system can cause changes in the charge distribution of the adsorbent and dye as a result of protonation and deprotonation reactions of functional groups [35][9]. The result of the optimization of the pH effect was shown in Figure 4(a).

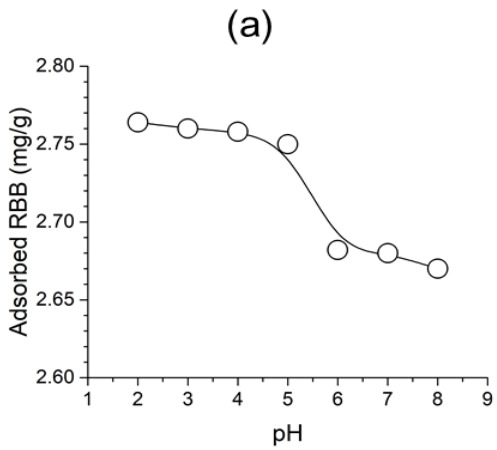

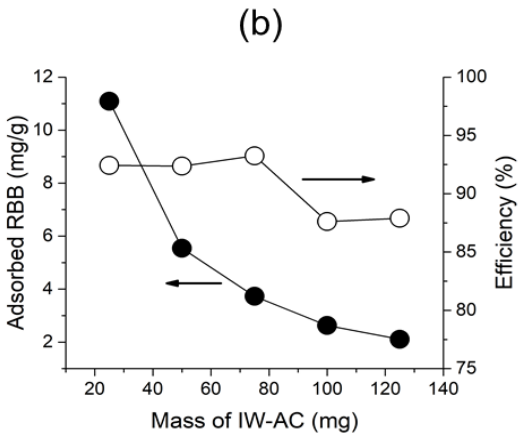

Figure 4. Effect of adsorbed RBB on IW-AC as a function of (a) pH and (b) mass of adsorbent.

The optimum pH observed in this work was 2.0. This occurs because of the protonation and de-protonation reactions of functional groups of activated carbon and RBB dye. At lower pH, the electrostatic interaction between positively charged IW-AC and negatively charged RBB dye interacts well to provide high adsorption efficiency [36]. Therefore, the efficiency and adsorption capacity of RBB on IW-AC decreased with the increasing pH of the solution. This is due to changes in the charge distribution on the surface of the IW-AC and RBB dye.Variation of the adsorbent mass aimed to determine the effective mass of IW-AC to adsorb RBB dye until it reached the equilibrium state. The adsorbed RBB on IW-AC as a function of IA-AC mass of adsorbent was shown in Figure 4(b).

Figure 4(b) shows that the adsorption efficiency increased with increasing mass IW-AC at 25-75 mg. The increase occurred because the increase in adsorbent mass made the availability of IW-AC active sites also increase. However, with IW-AC mass above 75 mg, the efficiency was decreased

due to equilibrium shifting [37]. Conversely, the adsorbed RBB per gram IW-AC was decreased as the mass of the IW-AC increased. The shift in the adsorption equilibrium can explain this. Therefore, when the adsorbent mass increases, the active sites on the surface of the adsorbent become unsaturated and cause the adsorbed RBB to decrease [37].

The proposed adsorption mechanism of RBB on IW-AC at low pH conditions is presented in Figure 5. In this condition, the number of H+ ions in the solution increases and protonates the carboxyl group of the IW-AC surface to become an electropositive –$COOH_2^+$ group. Meanwhile, RBB dye is dissociated to form an electronegative sulfonate group (–SO_3^-). Electrostatic interactions occurred between the positive charge (–$COOH_2^+$) IW-AC surface and the negative charge (-SO_3^-) of the RBB functional group. The H^+ ions in the solution also serve to bridge the bonds between the groups of the IW-AC surface and RBB dye molecules [38].

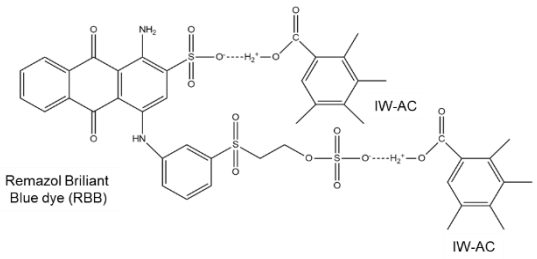

Figure 5. Schematic representation of the IW-AC interaction with RBB dye

4. Isotherm Study

Performance optimization of IW-AC conducted by applying the data of initial RPP concentration to the isotherm model: Langmuir [39] (Equation 5), Freundlich [40] (Equation 6), and Dubinin-Radushkevich/ D-R [41] (Equation 7).

$$\frac{C_e}{q_e} = \frac{1}{K_L b} + \frac{1}{b} C_e \quad (5)$$

$$\ln q_e = \ln B + \frac{1}{n} \ln C_e \quad (6)$$

$$\ln q_e = \ln q_D - B_D \varepsilon^2 \quad (7)$$

Where the *b* (mg/g) is the monolayer adsorption capacity, K_L (L/mol) is Langmuir equilibrium constant, *B* (mg/g) is the multilayer adsorption capacity, q_D (mg/g) is the D-R isotherm capacity, B_D (mol^2/J^2) relates to the free energy of RBB migration into the IW-AC surface, and ε (J^2/mol^2) is the Polanyi potential [ε = RT ln (1+1/C_e)].

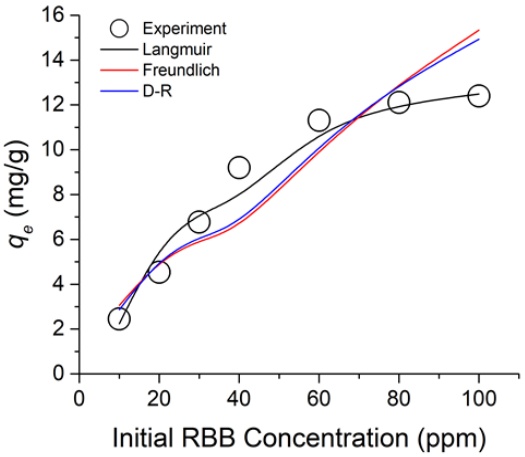

Figure 6. The suitability of the isotherm data to the Langmuir, Freundlich, and D-R isotherm model

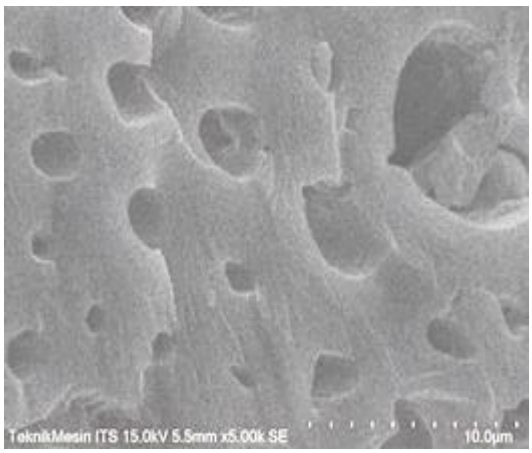

Figure 7. The FT-IR spectrum and SEM image of IW-AC after adsorbing RBB

Figure 6 shows the suitability of the isotherm data to the isotherm model, and the calculated value of the corresponding parameter was listed in Table 1. The adsorption of RBB was increased with increasing C_0 from 10 to 100 ppm. After that, the adsorption slowly reached equilibrium with no further RBB adsorption. By correlating the correlation coefficient (R^2) value of the isotherm models in Table 1, the Langmuir model show the best representative model for the sorption system, which indicate the monolayer adsorption with the capacity of 13.42 mg/g. This value was comparable to the previous RBB adsorption: Cassava dregs (16.88 mg/g) [38], coffee husk-based AC (66.76 mg/g) [36], and agro-industrial waste *Jatropha curcas* pods-AC (5.63 mg/g) [42].

The D-R isotherm is possible to predict the adsorption mechanism by calculated the adsorption energy (E_{D-R}). E_{D-R} can be calculated by $(2B_D)^{-1/2}$ if the value of E_{D-R} is <8 kJ/mol the adsorption type can be explained by physical adsorption, between 8 and 16 kJ/mol the adsorption type can be explained by ion exchange or electrostatic interaction, and >16 kJ/mol the adsorption type can be explained by stronger chemical adsorption [43], [44]. The calculated E_{D-R} found in this study was 13.39 kJ/mol. This indicates the ion exchange or electrostatic is the major mechanism of the RBB adsorption o IWAC.

FT-IR and SEM analysis can observe this mechanism after the RBB adsorption (Figure 7). The difference in functional groups between the FTIR spectrum of IW-AC before and after adsorption showed a shift in the wave number in the O–H, C–H aliphatic, C≡C, C=O, C=C, and C–H aromatic functional groups and the formation of new peaks indicating the bonding of C–O (1358 cm^{-1}) and S=O (1192 cm^{-1}) groups. The functional group above shows that RBB is completely adsorbed on the IW-AC surface more to the electrostatic interaction , as shown in Figure 5. In addition, the surface of the activated carbon in Figure 7 appeared smoother and flatter. This indicates that the adsorbed RBB on IW-AC. Further, after adsorption, the pore size after adsorption seems smaller (pore size: 0.71–8.85) than before.

Table 1. The isotherm parameter value of RBB adsorption on IW-AC

Langmuir			Freundlich			D-R		
b (mg/g)	*K* (L/mol)	R^2	*B* (mg/g)	*n*	R^2	q_D (mg/g)	B_D (mol^2/J^2)	R^2
13.42	157305.49	0.9971	285.78	2.60	0.8763	34.26	2.79×10^9	0.9045

5. Kinetics Study

Investigation of the corresponding kinetics parameter of RBB adsorption on IW-AC was conducted by applying kinetics data to the Lagergren / pseudo-first-order (Equation 8) [45] and Ho / pseudo-second-order (Equation 9) kinetics model [46]. In addition, the correlation of adsorption rate constant (k_a) and desorption rate constant (k_d) to the isotherm equilibrium constant (K) was investigated by the kinetics model proposed by Rusdiarso-Basuki-Santosa / RBS (Equation 10) [47], [48] model.

$$\ln(q_e - q_t) = \ln q_e - k_{Lag} t \quad (8)$$

$$\frac{t}{q_t} = \frac{1}{k_{Ho}\left(q_e^{\,2}\right)} + \frac{1}{q_e} t \quad (9)$$

$$\ln\left(\frac{C_0 C_b - x_e x}{x_e - x}\right) = k_a \left(\frac{C_0 C_b - x_e^{\,2}}{x_e}\right) t - \ln\left(\frac{x_e}{C_0 C_b}\right) \quad (10)$$

Where x (mol/L) and x_e (mol/L) are the amount of adsorbed RBB on the IW-AC's active site at time t and equilibrium, respectively. C_b (mol/L) is the concentration of monolayer Langmuir capacity (b). C_b is calculated from bw/v where w (g) is the mass of the IW-AC, and v (L) is the volume of RBB. k_{Lag} (min^{-1}), k_{Ho} (g/mol min), and k_a (L/mol min) are the Lagergren, Ho, and RBS rate constants, respectively. k_d (min^{-1}) denotes the desorption rate constant of RBS model.

Table 2. Kinetics parameter value of RBB adsorption on IW-AC

Lagergren	k_{Lag} (min^{-1})	0.0513
	$q_{e,\,calc}$ (mg/g)	1.26
	R^2	0.8947
Ho	k_{Ho} (g/mol min)	72933.53
	$q_{e,\,calc}$ (mg/g)	2.89
	R^2	0.9998
RBS	k_a (L/mol min)	372.64
	k_d (min^{-1})	0.0211
	$q_{e,\,calc}$ (mg/g)	1.33
	R^2	0.9011
Experiment	$q_{e,\,exp}$ (mg/g)	2.82

The adsorption rates of RBB on IW-AC has quickly occurred at the first 30 min and slowly continue until attained the equilibrium at 120 min (Figure 8a). The slight difference in concentration gradient may cause a slow step. The increasing RBB adsorption on IW-AC was observed due to the occupying a free site of IW-AC's active site, where there was the considerable free site of unsaturated that resulted in quick initial adsorption. After that, as times continue, the free sites got saturated reached the equilibrium. In this study, the adsorbed RBB on IW-AC was found to be 2.82 mg/g.

The application of the experimental data to the kinetics model in Equation (9)-(11) and the obtained corresponding parameter value were presented in Figure 8 and Table 2, respectively. Compared to Lagergren PFO (Figure 8b) and RBS (Figure 8d), the Ho PSO (Figure 8b) model was showed the best model to represent the RBB adsorption on IW-AC in this work. The Ho PSO's correlation coefficient value (0.999) was higher than other kinetics models, and the calculation of q_e ($q_{e,\,calc}$) of Ho (2.89 mg/g) (Table 2) was also the closest to the experimental q_e ($q_{e,\,exp}$ = 2.82 mg/g) in this work. This indicates that the adsorption process follows the pseudo-second-order mechanism.

Table 3. Comparison of the equilibrium constant (K) and adsorption energy E generated from Langmuir isotherm and RBS kinetics model.

Langmuir		RBS	
K_L (L/mol)	E_L (kJ/mol)	K_{RBS} (L/mol)	E_{RBS} (kJ/mol)
157305.49	29.64	17691.64	24.23

Further observation of the Ho PSO (k_{Ho}) and Lagergren PFO (k_{Lag}) adsorption rate constant is no triangulation method to examine these parameters. Therefore the proposed RBS kinetics models possible to generate the desorption rate constant (k_d) and through $K_{RBS}=k_a/k_d$ relationship, the Langmuir equilibrium constant (K_L) can be compared. The comparison result of the parameter was listed in Table 3. Thus, the predicted adsorption energy (E_{RBS} = 24.23 kJ/mol) is fairly comparable to the E_L (29.64 kJ/mol).

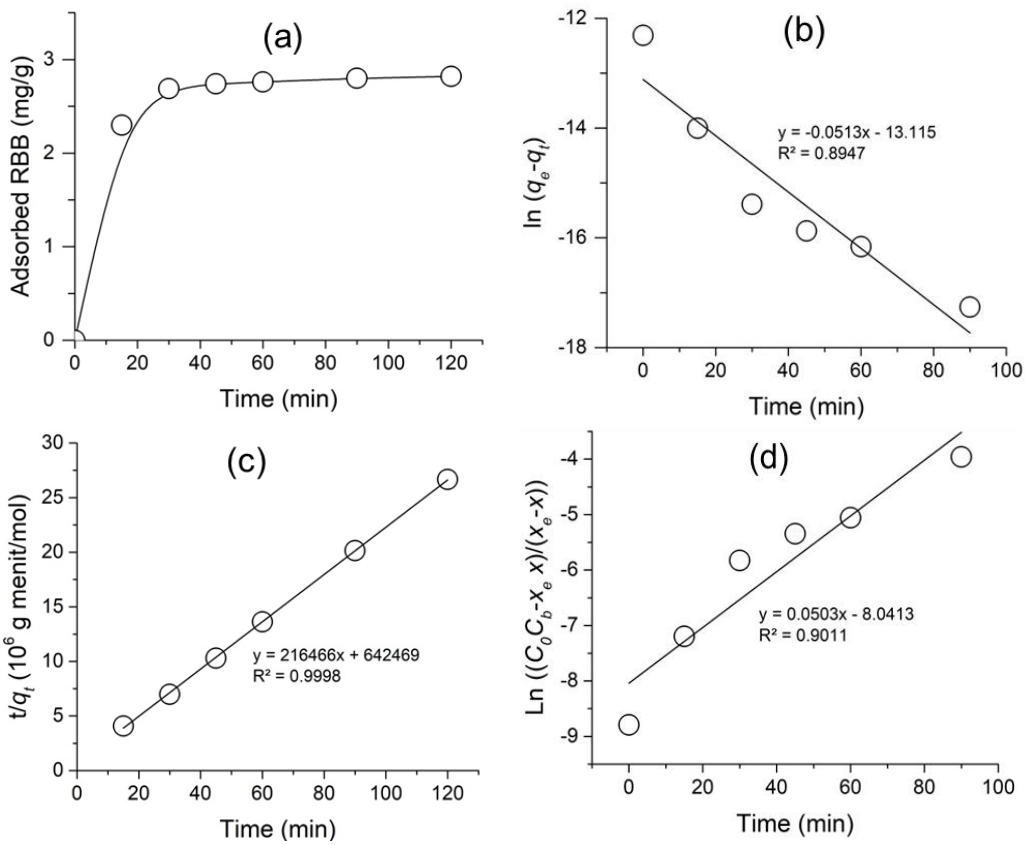

Figure 8. (a) Profile of adsorbed RBB as a function of time; Application of the experimental data to the kinetics model: (b) Lagergren PFO, (c) Ho PSO, and (d) RBS

CONCLUSION

Research on the synthesis of Ilalang weeds (*Imperata cylindrica*)-based activated carbon using KOH activator as green and low price RBB adsorbent has been successfully conducted. The success synthesis was evidently characterized by FT-IR and SEM instruments. The optimum condition of RBB adsorption occurred at low pH (2.0-4.0) and 75 mg of adsorbent dosage. Under the optimum condition, the monolayer adsorption capacity of RBB uptake was 13.42 mg/g with the D-R adsorption energy of 13.39 kJ/mol that indicates electrostatic interaction. Kinetics study of RBB uptake followed the Ho PSO kinetics mechanism.

ACKNOWLEDGEMENT

The authors thanks to Universitas Jambi through PTUPT Program (No Contract: 2653/UN21.18/PG/SPK/2020) for financing this work.

REFERENCES

[1] M. Behera, J. Nayak, S. Banerjee, S. Chakrabortty, and S. K. Tripathy, “A review on the treatment of textile industry waste effluents towards the development of efficient mitigation strategy: an integrated system design approach,” *J. Environ. Chem. Eng.*, p. 105277, 2021, doi: 10.1016/j.jece.2021.105277

[2] G. Kour, R. Kothari, R. Azam, P. K. Majhi, S. Dhar, D. Pathania, and V. V Tyagi, “Conducting Polymer Based Nanoadsorbents for Removal of

Heavy Metal Ions/Dyes from Wastewater," in *Advances in Hybrid Conducting Polymer Technology*, Springer, 2021, pp. 135–157. doi:10.1007/978-3-030-62090-5_7

[3] R. Kishor, D. Purchase, G. D. Saratale, R. G. Saratale, L. F. R. Ferreira, M. Bilal, R. Chandra, and R. N. Bharagava, "Ecotoxicological and health concerns of persistent coloring pollutants of textile industry wastewater and treatment approaches for environmental safety," *J. Environ. Chem. Eng.*, p. 105012, 2021, doi: 10.1016/j.jece.2020.105012

[4] M. Malakootian, K. Kannan, M. A. Gharaghani, A. Dehdarirad, A. Nasiri, Y. D. Shahamat, and H. Mahdizadeh, "Removal of metronidazole from wastewater by Fe/charcoal micro electrolysis fluidized bed reactor," *J. Environ. Chem. Eng.*, vol. 7, no. 6, p. 103457, 2019, doi: 10.1016/j.jece.2019.103457

[5] H. Te Hsu, S. S. Chen, and Y. S. Chen, "Removal of chromium(VI) and naphthalenesulfonate from textile wastewater by photocatalysis combining ionic exchange membrane processes," *Sep. Purif. Technol.*, vol. 80, no. 3, pp. 663–669, 2011, doi:10.1016/j.seppur.2011.06.032

[6] L. Bukman, N. R. C. Fernandes-Machado, W. Caetano, A. L. Tessaro, and N. Hioka, "Treatment of wastewater contaminated with ionic dyes: Liquid-liquid extraction induced by reversed micelle followed by photodegradation," *Sep. Purif. Technol.*, vol. 189, no. August, pp. 162–169, 2017, doi:10.1016/j.seppur.2017.08.004

[7] M. P. da Silva, A. C. A. de Souza, L. E. de Lima Ferreira, L. M. Pereira Neto, B. F. Nascimento, C. M. B. de Araújo, T. J. M. Fraga, M. A. da Motta Sobrinho, and M. G. Ghislandi, "Photodegradation of Reactive Black 5 and raw textile wastewater by heterogeneous photo-Fenton reaction using amino-Fe3O4-functionalized graphene oxide as nanocatalyst," *Environ. Adv.*, vol. 4, no. December 2020, p. 100064, 2021, doi:10.1016/j.envadv.2021.100064

[8] N. S. Naik, M. Padaki, S. Déon, and D. H. K. Murthy, "Novel poly (ionic liquid)-based anion exchange membranes for efficient and rapid acid recovery from industrial waste," *Chem. Eng. J.*, vol. 401, no. April, p. 126148, 2020, doi: 10.1016/j.cej.2020.126148

[9] R. Basuki, B. Rusdiarso, S. J. Santosa, and D. Siswanta, "Magnetite-Functionalized Horse Dung Humic Acid (HDHA) for the Uptake of Toxic Lead (II) from Artificial Wastewater," *Adsorpt. Sci. Technol.*, vol. 2021, no. 5523513, pp. 1–15, 2021, doi:10.1155/2021/5523513.

[10] N. Ngatijo, N. Gusmaini, R. Bemis, and R. Basuki, "Adsorpsi Methylene Blue pada Nanopartikel Magnetit tersalut Asam Humat: Kajian Isoterm dan Kinetika," *CHEESA Chem. Eng. Res. Artic.*, vol. 4, no. 1, pp. 51–64, 2021, doi:10.25273/cheesa.v4i1.8433.51-64

[11] Y. Zhou, M. Zhang, X. Wang, Q. Huang, Y. Min, T. Ma, and J. Niu, "Removal of crystal violet by a novel cellulose-based adsorbent: comparison with native cellulose," *Ind. Eng. Chem. Res.*, vol. 53, no. 13, pp. 5498–5506, 2014, doi: 10.3923/JBS.2007.222.230

[12] B. Rusdiarso and R. Basuki, "Stability Improvement of Humic Acid as Sorbent through Magnetite and Chitin Modification," *J. Kim. Sains dan Apl.*, vol. 23, no. 5, pp. 152–159, 2020, doi: 10.1021/ie404135y

[13] M. A. K. M. Hanafiah, W. S. W. Ngah, H. Zakaria, and S. C. Ibrahim, "Batch study of liquid-phase absorption of lead ions using lalang (Imperata cylindrica) leaf powder," *Journal of Biological Sciences*, vol. 7, no. 2. pp. 222–230, 2007. doi:10.14710/jksa.23.5.152-159

[14] T. Huda and T. K. Yulitaningtyas, "Kajian adsorpsi methylene blue menggunakan selulosa dari alang-

alang," *IJCA (Indonesian J. Chem. Anal.*, vol. 1, no. 01, pp. 9–19, 2018, doi: 10.20885/ijca.vol1.iss1.art2

[15] A. A. Erprihana and D. Hartanto, "Pembuatan Karbon Aktif Dari Kulit Jeruk Keprok (Citrus Reticulata) Untuk Adsorbsi Pewarna Remazol Brilliant Blue," *J. Bahan Alam Terbarukan*, vol. 3, no. 2, pp. 60–65, 2014, doi: 10.15294/jbat.v3i2.3699

[16] B. S. Pratama, "Konversi ampas tebu menjadi biochar dan karbon aktif untuk penyisihan Cr (VI)," *J. Rekayasa Bahan Alam dan Energi Berkelanjutan*, vol. 2, no. 1, pp. 7–12, 2018.
Google Scholar

[17] A. Arevalo-Gallegos, Z. Ahmad, M. Asgher, R. Parra-Saldivar, and H. M. N. Iqbal, "Lignocellulose: a sustainable material to produce value-added products with a zero waste approach—a review," *Int. J. Biol. Macromol.*, vol. 99, pp. 308–318, 2017, doi:10.1016/j.ijbiomac.2017.02.097

[18] L. Maulinda, Z. A. Nasrul, and D. N. Sari, "Pemanfaatan kulit singkong sebagai bahan baku karbon aktif," *J. Teknol. Kim. Unimal*, vol. 4, no. 2, pp. 11–19, 2017,
doi:10.29103/jtku.v4i2.69

[19] L. Efiyanti, S. A. Wati, and M. Maslahat, "Pembuatan dan Analisis Karbon Aktif dari Cangkang Buah Karet dengan Proses Kimia dan Fisika," *J. Ilmu Kehutan.*, vol. 14, no. 1, pp. 94–108, 2020,
doi: 10.22146/jik.5747

[20] E. Erawati and A. Fernando, "Pengaruh jenis aktivator dan ukuran karbon aktif terhadap pembuatan adsorbent dari serbik gergaji kayu sengon (Paraserianthes Falcataria)," *J. Integr. Proses*, vol. 7, no. 2, pp. 58–66, 2018.
doi:10.36055/jip.v7i2.3808

[21] M. F. P. Sari, P. Loekitowati, and R. Moehadi, "Penggunaan Karbon Aktif Dari Ampas Tebu Sebagai Adsorben Zat Warna Procion Merah Dari Industri Songket," *J. Pengelolaan Sumberd. Alam dan Lingkung. (Journal Nat. Resour. Environ. Manag.*, vol. 7, no. 1, pp. 37–40, 2017, doi:10.29244/jpsl.7.1.37-40

[22] A. Husin and A. Hasibuan, "Studi Pengaruh Variasi Konsentrasi Asam Posfat (H3PO4) dan Waktu Perendaman Karbon terhadap Karakteristik Karbon Aktif dari Kulit Durian," *J. Tek. Kim. USU*, vol. 9, no. 2, pp. 80–86, 2020,
doi: 10.32734/jtk.v9i2.3728

[23] L. Hakim and E. Sedyadi, "Synthesis and Characterization of Fe3O4 Composites Embeded on Coconut Shell Activated Carbon," *JKPK (Jurnal Kim. dan Pendidik. Kim.*, vol. 5, no. 3, pp. 245–253.
doi:10.20961/jkpk.v5i3.46543

[24] F. I. Nuria, M. Anwar, and D. Y. Purwaningsih, "Pembuatan Karbon Aktif dari Enceng Gondok," *J. TECNOSCIENZA*, vol. 5, no. 1, pp. 37–48, 2020.

[25] P. Kuptajit, N. Sano, K. Nakagawa, and T. Suzuki, "A study on pore formation of high surface area activated carbon prepared by microwave-induced plasma with KOH (MiWP-KOH) activation: Effect of temperature-elevation rate," *Chem. Eng. Process. - Process Intensif.*, vol. 167, no. June, p. 108511, 2021, doi: 10.1016/j.cep.2021.108511

[26] W. Chen, M. Gong, K. Li, M. Xia, Z. Chen, H. Xiao, Y. Fang, Y. Chen, H. Yang, and H. Chen, "Insight into KOH activation mechanism during biomass pyrolysis: Chemical reactions between O-containing groups and KOH," *Appl. Energy*, vol. 278, no. 115730, pp. 1–12, 2020, doi: 10.1016/j.apenergy.2020.115730

[27] J. Wang, S. Lei, and L. Liang, "Preparation of porous activated carbon from semi-coke by high temperature activation with KOH for the high-efficiency adsorption of aqueous tetracycline," *Appl. Surf. Sci.*, vol. 530, no. April, p. 147187, 2020,
doi:10.1016/j.apsusc.2020.147187

[28] F. Hanum, R. J. Gultom, and M. Simanjuntak, "Adsorpsi Zat Warna Metilen Biru dengan Karbon Aktif dari Kulit Durian Menggunakan KOH dan NAOH sebagai Aktivator," *J. Tek. Kim. USU*, vol. 6, no. 1, pp. 49–55, 2017, doi: 10.32734/jtk.v6i1.1565

[29] A. Khilya and A. T. Prasetya, "Optimasi Aplikasi Arang Aktif Alang-Alang dalam Menurunkan Kadar Cd2+ pada Larutan," *Indones. J. Chem. Sci.*, vol. 5, no. 1, 2016, doi: 10.15294/usej.v5i3.13185

[30] K. Elly, "Pemanfaatan cangkang kelapa sawit sebagai arang aktif," *J. Penelit. Ilmu-Ilmu Tek.*, vol. 8, no. 2, pp. 96–103, 2008.

[31] M. O. Esterlita and N. Herlina, "Pengaruh penambahan aktivator ZnCl2, KOH, dan H3PO4 dalam pembuatan karbon aktif dari pelepah aren (Arenga Pinnata)," *J. Tek. Kim. USU*, vol. 4, no. 1, pp. 47–52, 2015, doi:10.32734/jtk.v4i1.1460.

[32] T. S. Hui and M. A. A. Zaini, "Potassium hydroxide activation of activated carbon: A commentary," *Carbon Lett.*, vol. 16, no. 4, pp. 275–280, 2015, doi: 10.5714/CL.2015.16.4.275

[33] A. Hidayati, S. Kurniawan, N. W. Restu, and B. Ismuyanto, "Potensi ampas tebu sebagai alternatif bahan baku pembuatan karbon aktif," *Nat. B*, vol. 3, no. 4, pp. 311–317, 2016,

[34] Z. A. Nasution and S. M. Rambe, "Karakterisasi dan identifikasi gugus fungsi dari karbon cangkang kelapa sawit dengan metode methano-pyrolysis," *J. Din. Penelit. Ind.*, vol. 24, no. 2, pp. 108–113, 2013, doi:10.28959/jdpi.v24i2.530

[35] Z. Z. Zam, N. A. Limatahu, and N. J. Baturante, "Nitrate Adsorption capacity of Activated Gamalama Volcanic Ash," *JKPK (Jurnal Kim. dan Pendidik. Kim.*, vol. 6, no. 1, pp. 23-28, doi:10.20961/jkpk.v6i1.48462

[36] M. A. Ahmad and N. K. Rahman, "Equilibrium, kinetics and thermodynamic of Remazol Brilliant Orange 3R dye adsorption on coffee husk-based activated carbon," *Chem. Eng. J.*, vol. 170, no. 1, pp. 154–161, 2011, doi:10.1016/j.cej.2011.03.045

[37] S. Sy, D. Kurniawati, I. Lestari, H. Harmiwati, and M. Kasman, "Pengaruh pH dan dosis adsorben dari limbah lumpur aktif industri crumb rubber terhadap kapasitas penyerapan ion Cd (II) dan Zn (II)," *J. Litbang Ind.*, vol. 8, no. 2, pp. 95–104, 2018, doi:10.24960/jli.v8i2.4290.95-104

[38] A. W. K. Wahyuningsih, I. Ulfin, and S. Suprapto, "Pengaruh pH dan Waktu Kontak Pada Adsorpsi Remazol Brilliant Blue R Menggunakan Adsorben Ampas Singkong," *J. Sains dan Seni ITS*, vol. 7, no. 2, pp. 17–19, 2019, doi: 10.12962/j23373520.v7i2.30070

[39] I. Langmuir, "The Adsorption of Gases on Plane Surfaces of Mica," *J. Am. Chem. Soc.*, vol. 40, no. 9, pp. 1361–1403, 1918, doi:10.1021/ja02242a004

[40] H. Freundlich, "Uber die Adsorption in Losungen," *Zeitschrift für Phys. Chemie*, vol. 57, no. (1), pp. 385–470, 1960, doi: 10.1515/zpch-1907-572

[41] M. M. Dubinin and L. V. Radushkevich, "The equation of the characteristic curve of the activated charcoal USSR," *Proc. Acad. Sci. Phys. Chem. Sect.*, vol. 55, pp. 331–337, 1947.

[42] P. Sathishkumar, M. Arulkumar, and T. Palvannan, "Utilization of agro-industrial waste Jatropha curcas pods as an activated carbon for the adsorption of reactive dye Remazol Brilliant Blue R (RBBR)," *J. Clean. Prod.*, vol. 22, no. 1, pp. 67–75, 2012, doi: 10.1016/j.jclepro.2011.09.017

[43] P. Saha, S. Chowdhury, S. Gupta, and I. Kumar, "Insight into adsorption equilibrium, kinetics and thermodynamics of Malachite Green onto clayey soil of Indian origin," *Chem. Eng. J.*, vol. 165, no. 3, pp. 874–882, 2010, doi: 10.1016/j.cej.2010.10.048

[44] S. Shen, T. Pan, X. Liu, L. Yuan, Y. Zhang, J. Wang, and Z. Guo, "Adsorption of Pd(II) complexes from chloride solutions obtained by leaching chlorinated spent automotive catalysts on ion exchange resin Diaion WA21J," *J. Colloid Interface Sci.*, vol. 345, no. 1, pp. 12–18, 2010, doi:10.1016/j.jcis.2010.01.049.

[45] S. Lagergren, "Kungliga svenska vetenskapsakademiens," *Handlingar*, vol. 24, no. 4, pp. 1–39, 1898. doi:10.12691/ijebb-4-2-4

[46] Y. S. Ho and G. McKay, "Sorption of dye from aqueous solution by peat," *Chem. Eng. J.*, vol. 70, no. 2, pp. 115–124, 1998, doi: 10.1016/S0923-0467(98)00076-1

[47] B. Rusdiarso, R. Basuki, and S. J. Santosa, "Evaluation of Lagergren kinetics equation by using novel kinetics expression of sorption of Zn 2+ onto horse dung humic acid (HD-HA)," *Indones. J. Chem.*, vol. 16, no. 3, pp. 338–346, 2016, doi:10.22146/ijc.21151

[48] R. Basuki, Ngatijo, S. J. Santosa, and B. Rusdiarso, "Comparison the new kinetics equation of noncompetitive sorption Cd(II) and Zn(II) onto green sorbent horse dung humic acid (HD-HA)," *Bull. Chem. React. Eng. Catal.*, vol. 13, no. 3, pp. 475–488, 2018, doi:10.9767/bcrec.13.3.1774.475-488